Chinese Chemical Letters 33 (2022) 2757–2762

Contents lists available at ScienceDirect

Chinese Chemical Letters

journal homepage: www.elsevier.com/locate/cclet

Optimizing functional layer of cation exchange membrane by three-dimensional cross-linking quaternization for enhancing monovalent selectivity

Jiefeng Pan, Lei Zhao, Xiaohong Yu, Jiajing Dong, Lingling Liu, Xueting Zhao*, Lifen Liu*

College of Chemical Engineering, Zhejiang University of Technology, Hangzhou 310014, China

ARTICLE INFO

Article history:
Received 21 June 2021
Revised 18 August 2021
Accepted 30 August 2021
Available online 4 September 2021

Keywords:
Cation exchange membrane
Monovalent ion selectivity
Electrodialysis
Polypyrrole
Cross-linking

ABSTRACT

Monovalent cation perm-selective membrane (MCPMs) allow fast and selective transport of monovalent cations, and they are promisingly required for extraction of special ions, such as lithium extraction, acid recovery and sea salt production. Herein, we report a novel strategy to design the critical functional layers of MCPMs with both space charge repulsion and cross-linked dense screenability. The *in-situ* deposition polymerization of pyrrole was carried out on the surface of sulfonated polyphenyl sulfone (SPPSU) substrate membrane followed by cross-linking quaternization of the polypyrrole (PPy) layer with diiodinated functional molecules, thus, the membrane obtained more excellent selective permeability and stable transport properties of monovalent cations. It confirms that the designed PPy layers with charged surface and cross-linking structure improved the hydrophilicity, facilitated cation transport and increased ion flux. Meanwhile, for the dense PPy layer, the charged cross-linked structure endowed the functional layer with the synergistic characteristics of Donnan exclusion and pore size sieving for positively charged ions, which improved the monovalent cation perm-selectivity of the membranes. At a constant current density of 5.1 mA/cm^2, the optimal membrane exhibited superior perm-selectivity ($P_{Mg}^{Na} = 2.07$) and monovalent cation flux ($J_{Na^+} = 2.80 \times 10^{-8}$ mol cm^{-2} s^{-1}) during electrodialysis.

© 2021 Published by Elsevier B.V. on behalf of Chinese Chemical Society and Institute of Materia Medica, Chinese Academy of Medical Sciences.

Ion exchange membranes (IEMs) are the key component of electrodialysis (ED), diffusion dialysis (DD) and fuel cells, and they are pioneering ion separation materials for applications including clean production [1], pollution control [2], resource recovery [3,4] and energy storage and conversion [5,6]. Traditional IEMs mainly separate oppositely charged ions, *i.e.*, the separation between anions and cations. Nevertheless, with the transformation and upgrading of chemical production, water resources, energy and other traditional industries, ion exchange membrane technology also faces new opportunities and challenges. For example, the extraction of Li^+ from salt-lake solution with high Li/Mg ratio, the separation of H^+ from multivalent vanadium in the flow batteries, and the recovery of H^+ from waste acid solution containing heavy metals. Thus, selective electrodialysis technology with MCPMs had been proposed to meet actual industrial needs. As the core component of selective electrodialysis, the development of high performance MCPMs is a hot issue in the current field of separation materials.

The mono/multivalent ion selectivity is governed by the hydration energy difference of ions, the sieving effect and the Donnan exclusion based on the membrane structures and properties. Based on the above separation mechanisms, the preparation methods of MCPMs mainly include bulk modification and surface modification. For the bulk modifications, the internal sieving structure is constructed through controlling the compactness or increasing the repulsive force, such as covalent cross-linking, hot-pressing, acid-base interaction or positively charged dopant. However, the former may bring the high electrical resistance of the membranes and the latter did not significantly improve the perm-selectivity due to the limitation on the inherent properties of mosaic membrane. Some emerging technologies, such as electrospinning [7], constructing ion channels [8] and introducing porous structure [9–11] in the membranes, could prepare MCMPs with preferable properties. However, the complex design and preparation process limit their further application in industry. At the same time, surface modification has been proved to be one of the most effective modification strategies.

Surface modification is adopted to achieve selective transport of monovalent ions by constructing an ultrathin and selective functional layer (compact, hydrophobic and charged). In this way, only

* Corresponding authors.
E-mail addresses: zhaoxt@zjut.edu.cn (X. Zhao), lifenliu@zjut.edu.cn (L. Liu).

https://doi.org/10.1016/j.cclet.2021.08.121
1001-8417/© 2021 Published by Elsevier B.V. on behalf of Chinese Chemical Society and Institute of Materia Medica, Chinese Academy of Medical Sciences.

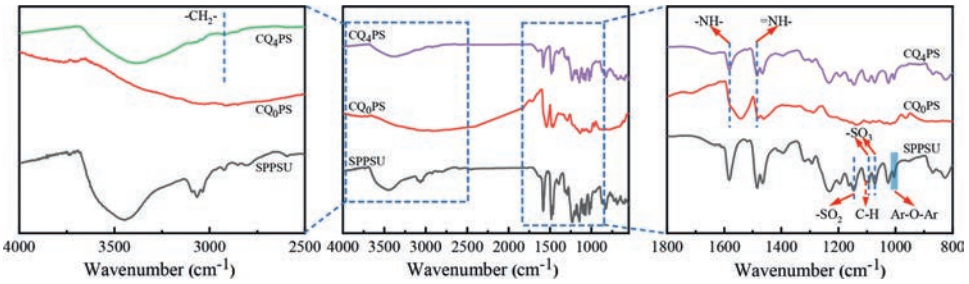

Fig. 1. The FT-IR spectra for SPPSU, CQ_0PS and CQ_4PS. The leftmost and rightmost figures are the enlargement of corresponding center figure.

the surface of the membrane is decorated with a thin functional layer, which is different from the bulk modification in the membrane matrix. And then high perm-selectivity is obtained due to the increased compactness of the membrane surface and/or the addition of an oppositely charged layer, such as polyaniline, polypyrrole, polyamide, dopamine and chitosan [12–20]. Among them, polyaniline and polypyrrole as prominent and well-studied conductive polymers, are naturally endowed with unique characteristics like the ease of preparation, environmental sustainability, and high electrical conductivity. In our previous work [21], polyaniline was firstly employed as a functional layer on the substrate membrane surface, and then the polyaniline layer was quaternized with CH_3I to prepare a series of MCPMs with varied positive charge density. The positive charge density on the surface of the modified membrane aroused with the increase of quaternization degrees, blocking the multivalent cations transport and maintaining the passage of monovalent cations. However, the high surface charge density inhibited ion permeation, resulting in lower ion flux. Furthermore, in order to stabilize inner cavities (ion transport channel), highly rigid polymer networks must be constructed to prevent the collapse of polymer chains into a nonporous dense state which results in loss of perm-selectivity [22].

Inspired by the hyper-crosslinked polymers networks [23–25], we proposed a novel strategy to engneer the three-dimensional cross-linked functional layer (separation layer) on the surface of cation exchange membrane (CEM). A series of MCPMs were prepared *via* quaternization of PPy modification layer with diiodinated functional molecules. Taking advantage of the cross-linking and quaternization characteristic of diiodinated functional molecules, the compactness (formation of crosslinking network) and surface charge of the functional layer were optimized. Morphological observations, chemical composition analysis, zeta potential measurements and the other related electrochemical characterizations were performed to investigate the effects of different quaternization reagents. More specifically, the electrodialysis experiment with respect to Na^+/Mg^{2+} system was conducted to evaluate the monovalent cation perm-selectivity of the MCPMs.

In order to construct three-dimensional cross-linked quaternized layer, PPy was deposited on CEM (SPPSU, some basic information about the substrate membrane are shown in Table S2 (Supporting information)) by *in-situ* chemical oxidative polymerization, and then the PPy layer was quaternized by diiodinated functional molecules (linear molecules with different carbon content) to form a cross-linked positively charged layer (Fig. S2 in Supporting information). The compactness and the positively charged exclusion of the functional layers were utilized to achieve the separation of monovalent and divalent cations.

The reaction process of the functional layer was similar to interfacial oxidative polymerization [26]. The ethanol solution of pyrrole was poured into the side of the substrate membrane containing $FeCl_3$ solution (Fig. S2a). When the oxidant (Fe^{3+}) in the aqueous phase contacted with the pyrrole monomer in the ethanol phase at the interface, the pyrrole monomer generated free radical cation under the catalytic oxidation of Fe^{3+}, and then the polymerization reaction stepwisely occurred between a radical cation and close pyrrole monomer or oligomer chain [27]. After polymerization, the membrane with a PPy layer (Fig. S2b) was immersed in ethanol solution of linear diiodine with different number of carbon atoms and thus quaternization and cross-linking reaction occurred between pyrrole and linear diiodinated molecules to obtain MCPMs (Fig. S2c). Herein, the hydrophilicity and swelling will be controlled by the as-fromed charged cross-linking structure, which will be useful to regulate cationic perm-selectivity and flux.

In order to understand the chemical structure of the functional layer on the membrane surface, the ATR-FTIR spectroscopic analysis was conducted and the results were shown in Fig. 1. The characteristic absorption peaks of substrate membrane (SPPSU) were as follows: 1007 cm^{-1} (Ar-O-Ar linkage), 1060 cm^{-1} and 1095 cm^{-1} (symmetric and asymmetric stretching peaks of the sulfonate group), 1150 cm^{-1} ($-SO_2$ symmetric stretching peak) and 1107 cm^{-1} (para in-plane aromatic C–H bond peak) [21,28]. The characteristic absorption of amino group (1590 cm^{-1}) and imino group (1480 cm^{-1}) of PPy can be observed after the formation of PPy layer by *in-situ* deposition polymerization [21,29,30]. A positively charged PPy layer was formed after quaternization reaction. The $-CH_2-$ (2923 cm^{-1}) stretching vibration was observed in the ATR-FTIR spectrum of CQ_4PS, which confirmed the occurrence of quaternization reaction.

To further investigate the chemical compositions of the membrane functional layer, the elemental composition and content of CQ_0PS and CQ_4PS were determined by XPS, respectively. Fig. 2a shows the presence of the expected C, N, O and S elements. C, N and O elements were the critical elements contained in the quaternized PPy layer, and S was the characteristic element of the substrate membrane. The peaks of CQ_nPS at 298.23 eV, 405.61 eV, 545.23 eV and 172.56 eV represented C 1s, N 1s, O 1s, S 2p, respectively. The XPS spectra of N element were analyzed by peak fitting to determine the states of N element, as shown in Figs. S3a and b (Supporting information) [31–33]. After computational analysis, Table S3 (Supporting information) shows the specific contributions of the N elements to the total N 1s in the three states. Compared with CQ_0PS (without quaternization), the N^+ percentages of CQ_4PS increased from 11.76% to 30.44%. The increasement of N^+ content on the membrane surface indicated the successful introduction of the positive charge on the PPy layer surface after quaternization. Fig. 2b shows the atomic concentrations and mass concentrations of C 1s, N 1s and I 3d in CQ_4PS. The atomic concentrations of C 1s, N 1s and I 3d are 89.54%, 10.45% and 0.01% respectively. It was observed that the content of N^+ is much higher than that of I 3d, which confirms the formation of cross-linking structure.

The effect of the cross-linking modification on the membrane surface morphology was investigated by SEM and TEM. Fig. 3 shows the surface and cross-section SEM images of the substrate membrane and modified membranes (CQ_0PS and CQ_4PS). Different

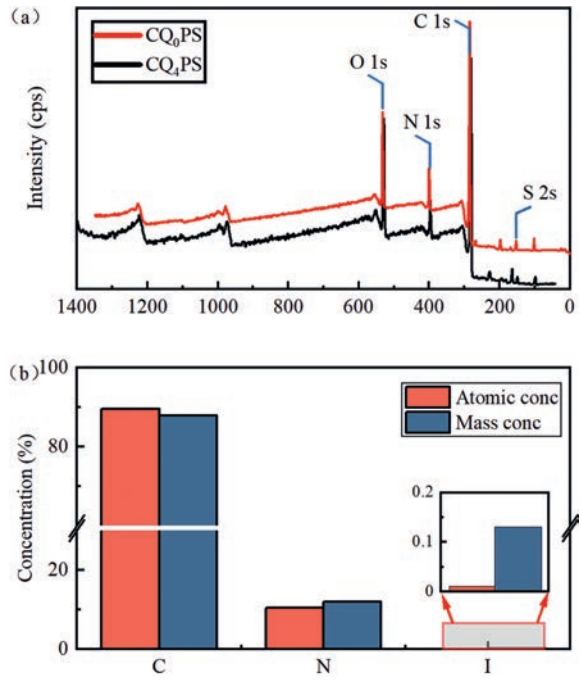

Fig. 2. XPS wide scan spectra (a); Atomic concentrations and mass concentrations of C 1s, N 1s and I 3d of CQ_4PS (b).

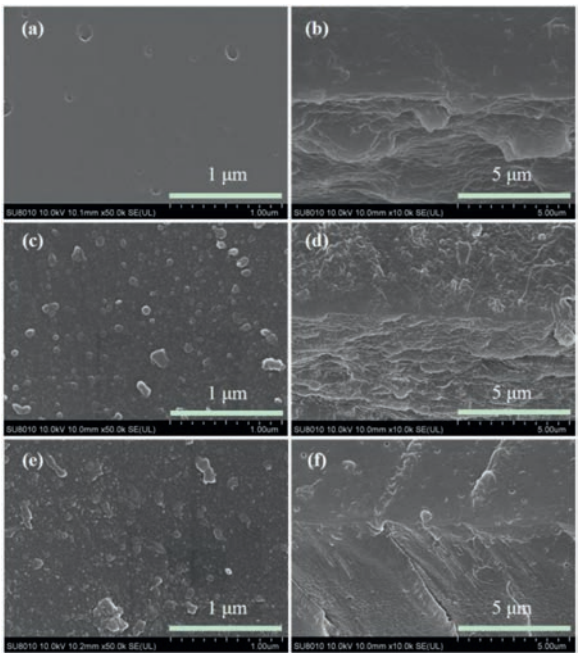

Fig. 3. SEM images of the surface of SPPSU (a), CQ_0PS (c), CQ_4PS (e); SEM cross-section images of SPPSU (b), CQ_0PS (d), CQ_4PS (f).

from the original smooth surface of substrate membrane (Fig. 3a), granular bumps were formed on the surface of the substrate membrane after *in-situ* deposition polymerization of pyrrole (Fig. 3c and Fig. S4b in Supporting information). Subsequently, the granule size became smaller after cross-linking quaternization modification, and the PPy layer was smoother and denser (Fig. 3e and Fig. S4c in Supporting information). It might be ascribed to the winding of cross-linking structure, which made the particles shrink and disperse more evenly. It is difficult to find the obvious interface from the SEM cross-section images (Figs. 3b, d and f), which indicated the close joint of the membrane and functional layer. Furthermore, TEM analysis of the modified membrane was carried out. As shown in Fig. S4a (Supporting information), CQ_0PS had a thin PPy layer (around 50 nm). There was excellent contact between the PPy layer and the substrate membrane, and no signs of delamination were found. This can be attributed to the continuous polymerization of pyrrole from outer surface of substrate membrane to the thin skin layer inside the substrate membrane and the tethering of the cross-linked structure.

For further observation of the surface microstructure of the modified membranes, AFM was used to detect the surface roughness after quaternization. As shown in Fig. S5 (Supporting information), the surface of CQ_nPS membranes were covered by tightly arranged PPy particles, which were consistent with particles distribution observed by SEM. The roughness of CQ_2PS to CQ_8PS decreased in turn, with the value of 6.03 nm, 5.60 nm, 5.10 nm and 5.43 nm, respectively. Meanwhile, the roughness of the cross-linked quaternized sample was significantly reduced relative to that of the unquaternized sample (CQ_0PS, R^a = 10.39 nm). The results indicated that the cross-linking quaternization modification would reduce the relative roughness of the membrane surface, and the increase of the carbon chains of the cross-linker would also reduce the relative roughness. This resulted from the cross-linking effect of diiodinated functional molecules and the transformation of linear molecular chain into three-dimensional network structure molecules upon cross-linking, affecting the arrangement order and regularity of the PPy molecules. As a result, the free interpenetration between molecular chains reduced and the arrangement order and regularity of the molecules were affected. To some degree, the longer carbon chain segments of the introduced diiodinated functional molecules would fill the previously formed valleys on the surfaces, smoothing the membrane surface, and thus, the peak-to-valley difference became smaller and the roughness reduced [34,35].

The surface charge of ion exchange membrane directly affects the Donnan repulsion between cations and membrane, and then may further determine the perm-selectivity of membrane to some extent. Therefore, the electrokinetic potential of the membrane surface was measured to characterize the surficial electrical charge properties. It can be seen from Fig. S6a (Supporting information) that the zeta potential values of CQ_0PS at three pH states were −1.03 mV, −0.68 mV and −0.75 mV respectively, which indicated that the PPy layer (without quaternization) was negatively charged. While the zeta potential values of the modified membranes all increased after the quaternization reaction, which was attributed to the increased positive charge density on the surface of the modified membranes resulted from the formation of quaternary ammonium groups by the quaternization reaction. After treatment with quaternization reagents with different carbon contents, the zeta potentials of membranes increased first and then decreased from CQ_2PS to CQ_8PS, which indicated that the carbon content of quaternization reagents had a large effect on the degree of quaternization. When the carbon content was low, there may be no suitable reaction site due to the limitation of spatial distance, resulting in low degree of cross-linking and quaternization. However, when the carbon content was high, it was difficult for diiodinated molecules to enter the PPy layer, which led to the decrease of the degree of quaternization reaction.

Water contact angle for the modified membranes was measured to investigate the change valuation of the hydrophobicity of the membranes surface. The water contact angle is primarily controlled by hydrophilic component of the membrane and surface roughness. The roughness of the membranes decreased after quaternization, while the difference in roughness of the different quaternized membranes was small according to Fig. S5 (Supporting information). Therefore, the contact angle of quaternized membrane was mainly affected by hydrophilicity. As shown in Fig. S6b

(Supporting information), the water contact angles of CQ_nPS are 81.9°, 93.6°, 85.9°, 86.7° and 99.3°, respectively. With the increase of carbon content of quaternization reagent, the water contact angle first decreased and then increased, which can be attributed to different degree of ammonium reaction and the grafting of carbon chain. With the increase of carbon content, the yield of ammonium decreased. CQ_0PS showed hydrophilic characteristic. The carbon chains introduced by cross-linking quaternization could enhance the hydrophobicity of the PPy surface. The contact angle of CQ_2PS surface was very high could be due to more carbon chains grafting and the tertiary ammonium without charge forming (The surface charge of CQ_2PS increases slightly) [23]. The large contact angle of CQ_8PS resulted from the longer grafted carbon chains.

Fig. S7 in Supporting information shows the ion exchange capacities of the substrate and modified membranes. The IEC of the substrate membrane and CQ_nPS membranes are 1.54 mmol/g, 1.49 mmol/g, 1.30 mmol/g, 1.34 mmol/g, 1.37 mmol/g and 1.33 mmol/g, respectively. Due to the polymerization of pyrrole on the surface of SPPSU membrane, the dry weight of the membrane increased and would result in slightly decreasing IEC of CQ_0PS. After the quaternization reaction, the sulfonic groups and quaternary ammonium groups in the functional layer were neutralized by electrostatic interaction, which reduced the amount of NaOH used in acid-base titration. While the introduction of quaternization reagents with different carbon content increased the W_{dry}, which further decreased the IEC of the modified membranes.

C-V curves are a vital tool to characterize the electrochemical behavior of ion exchange membranes over a wide range of currents. The C-V curves of ion exchange membranes are usually display three regions, *i.e.*, ohmic region, plateau region and over limit region. Fig. S8a (Supporting information) shows the C-V curves of the substrate membrane and modified membranes, which exhibit distinct three different regions. The limiting current density of CQ_nPS membranes were 68.12 mA/cm^2, 57.25 mA/cm^2, 6.87 mA/cm^2, 63.36 mA/cm^2, and 67.61 mA/cm^2 (Fig. S8b in Supporting information), respectively. (The limiting current density of CQ_4PS was obtained by analyzing the 1st derivative of the transmembrane voltage drop *vs*. the applied current (dE/di) as a function of current density.) The variation trend of limiting current density was consistent with water contact angle and opposite to zeta potential. This phenomenon was attributed to the positive charge on the functional layer as well as the dense cross-linked structure that limited the transport of cations. The limiting current density of CQ_4PS was much smaller than that of other membranes, and the zeta potential of CQ_4PS was also very high, which suggested that the positively charged functional layer have increased the concentration polarization. Owing to the presence of an additional diffusion barrier at the interface between the substrate membrane and functional layer, such polymer composite membranes were characterized by lower values of the limiting current.

Membrane area resistance is one of the most important parameters that reflect the performance of ion exchange membrane. *In-situ* deposition polymerization and cross-linking quaternization can change the resistance of the membrane and affect the electrochemical behavior of the membrane. Fig. S8c (Supporting information) shows the increased resistance value of the modified membrane compared with the substrate membrane (the increased resistance value of the SPPSU was 0). The area resistance of substrate membrane was 4.23 Ω cm^2, and the resistance of the modified membrane (CQ_0PS) increased by 0.89 Ω cm^2 after the *in-situ* deposition polymerization of pyrrole. The small increase value could be attributed to the conductive nature of the PPy itself. However, the resistance of the membrane increased greatly after cross-linking quaternization reaction, which resulted from the cross-linking of diiodinated functional molecules. Consequently, the functional layer became denser and it was difficult for cations

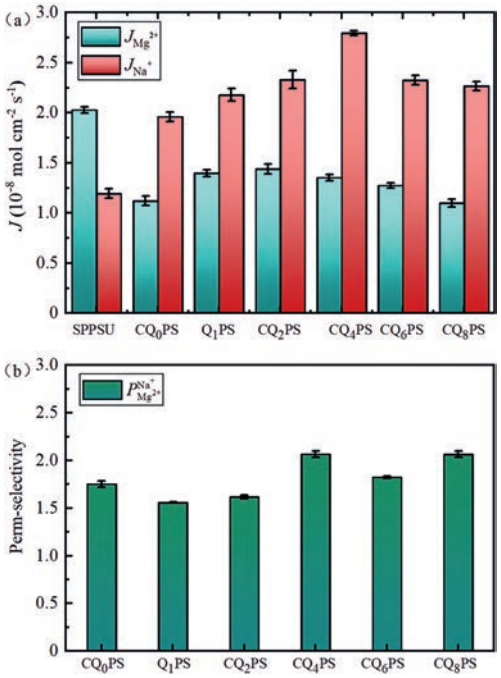

Fig. 4. The flux (a) and perm-selectivity (b) of substate and modificated membranes in concentrated chamber after 1 h.

to cross the functional layer. In addition, the increase of quaternary ammonium groups on the membrane surface also limited the ion transport due to Donnan exclusion. With the increase of carbon content of cross-linking agent, the increase value of the membrane area resistance first increased and then decreased, which was related to the degree of cross-linking quaternization of PPy layer.

The membranes were characterized in a binary mixture (Na^+/Mg^{2+}) to evaluate the perm-selective separation performance of substrate membrane and modified membranes using an ED setup in terms of perm-selectivity and ion flux. As shown in Fig. 4a, for SPPSU membrane, the electrostatic attraction of the fixed sulfonic group in the membrane to Mg^{2+} was greater than Na^+, which made Mg^{2+} much easier to occupy the adsorption site, and thus the transport of Na^+ was inhibited to a certain extent. As a result, the Mg^{2+} flux is slightly higher than that of Na^+. When the surface of SPPSU was covered with a dense PPy layer, the electrostatic attraction advantage of sulfonic acid groups to Mg^{2+} disappeared. The sieving effect of dense PPy layer on Na^+ and Mg^{2+} dominated the ion flux of the modified membrane due to the difference in hydrated radius (Table S4 in Supporting information) [36–39]. The Mg^{2+} transport with larger hydrated ionic radius was hindered by the dense functional layer at this time, resulting in a drastically reduced flux. The transport competition of Mg^{2+} was weakened and the Na^+ flux increased. After quaternization, the introduced positive charges generated greater Donnan exclusion force on divalent Mg^{2+} compared with monovalent Na^+ and the transport hindrance observed in divalent ions was enhanced. Meanwhile, the flux of Na^+ and Mg^{2+} increased first and then decreased with the increase of carbon content of quaternization reagents, which was consistent with the change of hydrophobicity of PPy layer. According to previous studies, the hydrophilicity of IEMs and the hydration energy of cations have an important role in the perm-selectivity of CEMs. The cations with a large Gibbs hydration energy are more affected by the hydrophobicity of the membrane surface, hence it is more difficult to cross the functional layer [31,38,40]. Besides, the positive charge density on the surface of CQ_nPS first increased and then decreased, thus, the Donnan repulsion force of the pos-

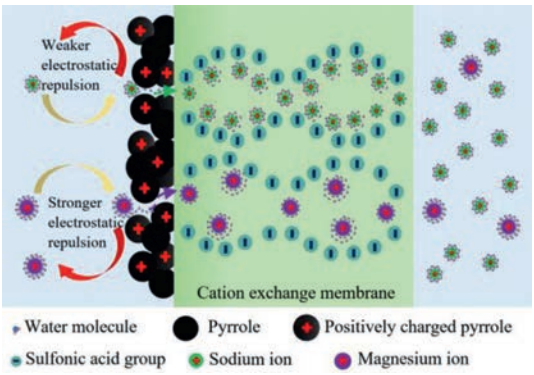

Fig. 5. Schematic diagram of CQ_nPS membrane structure and ion separation process.

itively charged functional layer on Mg^{2+} ions enhanced first and then weakened. As a consequence, the perm-selectivity increased first and then decreased (Fig. 4b). The Na^+/Mg^{2+} perm-selectivity of the optimal CQ_4PS membrane was 2.07. Moreover, as the perm-selectivity of MCPMs and ion flux from published papers shown in Table S5, the optimal CQ_4PS membrane had a considerable perm-selectivity and Na^+ flux.

The transport schematic diagram of Na^+ and Mg^{2+} ions across the membrane is shown in Fig. 5. Na^+ and Mg^{2+} in the diluted chamber form hydrated ions with different hydration layers due to electrostatic interaction (ion-dipole interaction) with water molecules. Hydrated Na^+ and Mg^{2+} migrated to the functional layer (facing the anode) driven by an electric field. When Na^+ and Mg^{2+} were close to the functional layer, their migration was blocked due to the Donan exclusion of the positively charged functional layer. The divalent Mg^{2+} was subject to stronger Donnan exclusion because it carried more charges than Na^+, *i.e.*, Mg^{2+} suffered from higher electrostatic barrier and stronger transport hindrance. Moreover, the cross-linking of the PPy layer endowed the functional layer with a more compact structure, and the sieving effect began to work when the ions overcome the electrostatic barrier to reach the gaps of the functional layer. In order to pass through the functional layer more easily, the ion was partially dehydrated to adapt to the pore size. The reported ionic hydrated radii vary in literatures, thus, which value of the effective ionic hydrated radii to choose is very important, and the ionic Stokes radii are also adopted [41–43]. However, no matter the ionic Stokes radii or the ionic hydrated radii, there was no doubt that the sizes of Na^+ and Mg^{2+} are different (Table S4). Compared with Na^+ with smaller radius, narrow functional layer channels showed stronger hindrance to Mg^{2+}. Taken together, the synergistic effect of Donnan exclusion and size sieving finally led to a lower flux of Mg^{2+} than Na^+, and the monovalent cation perm-selectivity of CQ_nPS membranes improved.

When the Na^+ and Mg^{2+} broke through the Donnan exclusion of the functional layer and the hindrance of the narrow pore channel, they reached the interface between the functional layer and the substrate membrane, and then entered the SPPSU membrane *via* water channels. The substrate membrane was composed of hydrophobic polyphenyl sulfone backbone and sulfonic acid groups on the backbone. Hydrophilic sulfonic acid groups formed clusters by self-organization, and absorbed water from the environment. As a result, there was an extended network of pores and channels filled with water in the membrane, and fixed sulfonic acid groups were localized on the pore walls. Due to the electrostatic interaction, most of the cations are located in a thin Debye layer near the pore walls. The high field strength in the Debye layer leads to the anion displacement from it, and this layer performs predominantly selective cationic transport [44,45]. Once some of the Mg^{2+} entered the membrane matrix, stronger binding of divalent Mg^{2+} with sulfonic groups decreased the available sites for Na^+ transport [37]. However, due to the block of the functional layer, the entry of magnesium ions was limited, so the competition of transport sites did not play a dominant role in perm-selectivity. Na^+ and Mg^{2+} gradually migrated from the inner membrane to the outer membrane and reached the concentrated chamber *via* the interaction with sulfonic groups on the water channel wall.

Fig. S9 (Supporting information) shows the perm-selectivity of CQ_4PS membrane for Na^+ and Mg^{2+} ions varied with the testing time. It was observed that the perm-selectivity fluctuated slightly around 2, indicating that no detachment happened during the tests. Probably, the formation of three-dimensional cross-linked structure can well consolidate the PPy layer, which contributed greatly to the stable MCPM at a fixed current density. Therefore, the excellent stability of CQ_4PS implied the potential for long-term electrodialysis process.

In this work, the novel monovalent cation perm-selective membranes were prepared *via in-situ* deposition polymerization of pyrrole on the surface of SPPSU substrate membrane followed by cross-linking quaternization of the PPy layer with diiodinated functional molecules. The successful preparation of MCPMs was verified by FTIR, XPS and SEM. The charge density and compactness of the functional layer were enhanced by the cross-linking and quaternization properties of diiodinated functional molecules. The results showed that the membrane prepared using 1,4-diiodobutane had higher charge density and lower hydrophobicity. The increased charge density of the membrane surface and the dense cross-linked structure work together, so that the limiting current density of the membrane decreased and the resistance increased. The Donnan exclusion and size sieving of the functional layer had a great adverse effect on the transport of Mg^{2+}, which resulted in the flux of Na^+ of the optimal CQ_4PS membrane is 2.80×10^{-8} mol cm^{-2} s^{-1}, and the perm-selectivity (Na^+/Mg^{2+}) of the CQ_4PS membrane is 2.07. The cross-linking modification strategy in this work is simple and feasible. It is expected to prepare MCPMs with higher selectivity and long-term stability *via* further study on the cross-linking structure.

Declaration of competing interest

The authors declare that they have no conflict of interest.

Acknowledgments

This research was supported by the Public Welfare Project of the Science and Technology Committee of Zhejiang Province (No. LGF20B060002), the China Postdoctoral Science Foundation funded project (No. 2016M601964), Provincial Key R&D Program of Zhejiang Province (No. 2019C03094) and the National Natural Science Foundation of China (Nos. 22075246 and 21776253).

Supplementary materials

Supplementary material associated with this article can be found, in the online version, at doi:10.1016/j.cclet.2021.08.121.

References

[1] B. Pan, H. Du, S. Wang, et al., J. Clean. Prod. 239 (2019) 118–129.
[2] A. Abou-Shady, Chem. Eng. J. 323 (2017) 1–18.
[3] L. Wang, M. Liu, J. Zhao, L. Yinlin, L. Nanwen, J. Mater. Chem. A 6 (2018) 22940–22950.
[4] W.G. Ji, N. Ul Afsar, B. Wu, et al., J. Membr. Sci. 590 (2019) 117267.
[5] A.H. Avci, T. Rijnaarts, E. Fontananova, et al., J. Membr. Sci. 595 (2020) 117585.
[6] P. Zuo, Y. Li, A. Wang, et al., Angew. Chem. Int. Ed. 59 (2020) 9564–9573.
[7] L. Hou, J. Pan, D. Yu, et al., J. Membr. Sci. 528 (2017) 243–250.

[8] L. Ge, X. Liu, G. Wang, et al., J. Membr. Sci. 475 (2015) 273–280.
[9] L. Ge, A.N. Mondal, X. Liu, et al., J. Membr. Sci. 536 (2017) 11–18.
[10] F.M. Sheng, L.X. Hou, X.X. Wang, et al., J. Membr. Sci. 594 (2020) 117453.
[11] L. Shu, N. Wang, C. Zhao, et al., ACS Sustain. Chem. Eng. 7 (2018) 2728–2738.
[12] X. Cheng, S. Ding, J. Guo, et al., J. Membr. Sci. 536 (2017) 19–27.
[13] H. Farrokhzad, M.R. Moghbeli, T. Van Gerven, B. van der Bruggen, React. Funct. Polym. 86 (2015) 161–167.
[14] L. Hou, B. Wu, D. Yu, et al., J. Membr. Sci. 557 (2018) 49–57.
[15] Y. Hu, M. Wang, D. Wang, X. Gao, C. Gao, J. Membr. Sci. 319 (2008) 5–9.
[16] J. Li, S. Yuan, J. Wang, et al., J. Membr. Sci. 553 (2018) 139–150.
[17] M.A. Shehzad, Y. Wang, A. Yasmin, et al., Angew. Chem. Int. Ed. 58 (2019) 12646–12654.
[18] X.G. Teng, M.R. Wang, G.W. Li, J.C. Dai, React. Funct. Polym. 157 (2020) 104777.
[19] S. Yang, Y. Liu, J. Liao, et al., ACS Appl. Mater. Interfaces 11 (2019) 17730–17741.
[20] Z. Yuan, Q. Dai, Y. Zhao, et al., J. Mater. Chem A (4) (2016) 12955–12962.
[21] X. Pang, Y.Y. Tao, Y.Q. Xu, et al., J. Membr. Sci. 595 (2020) 117544.
[22] L. Tan, B. Tan, Chem. Soc. Rev. 46 (2017) 3322–3356.
[23] J. Germain, J.M. Frechet, F. Svec, Chem. Commun. (2009) 1526–1528.
[24] J. Germain, J.M.J. Frechet, F. Svec, J. Mater. Chem. 17 (2007) 4989–4997.
[25] Y. Luo, B. Li, W. Wang, K. Wu, B. Tan, Adv. Mater. 24 (2012) 5703–5707.
[26] F. Zhang, J.B. Fan, S. Wang, Angew. Chem. Int. Ed. 59 (2020) 21840–21856.
[27] Y. Tan, K. Ghandi, Synth. Met. 175 (2013) 183–191.
[28] Y. Devrim, Electrochim. Acta 146 (2014) 741–751.
[29] B. Murugesan, N. Pandiyan, J. Sonamuthu, S. Samayanan, S. Mahalingam, Adv. Powder Technol. 29 (2018) 3173–3182.
[30] N. Wang, G. Li, Z. Yu, X. Zhang, X. Qi, Carbohydr. Polym. 127 (2015) 332–339.
[31] X. Pang, X.H. Yu, Y.B. He, et al., Sep. Purif. Technol. 270 (2021) 118768.
[32] M. Qiao, X. Lei, Y. Ma, et al., Ind. Eng. Chem. Res. 55 (2016) 6263–6275.
[33] N. Velhal, N.D. Patil, G. Kulkarni, et al., J. Alloys Compd. 777 (2019) 627–637.
[34] H. Liu, H. Ruan, Y. Zhao, et al., J. Membr. Sci. 543 (2017) 310–318.
[35] L.F. Ren, X.D. Ma, J. Zhang, T.T. Qiang, Polymer 194 (2020) 122370.
[36] L. Ge, B. Wu, D. Yu, et al., Chin. J. Chem. Eng. 25 (2017) 1606–1615.
[37] T. Luo, S. Abdu, M. Wessling, J. Membr. Sci. 555 (2018) 429–454.
[38] B. Tansel, Sep. Purif. Technol. 86 (2012) 119–126.
[39] T. Xu, M.A. Shehzad, X. Wang, et al., Nano-Micro Lett. 12 (2020) 51.
[40] R. Epsztein, E. Shaulsky, M. Qin, M. Elimelech, J. Membr. Sci. 580 (2019) 316–326.
[41] N.C. Nguyen, S.S. Chen, H.T. Hsu, C.W. Li, Desalination 328 (2013) 51–57.
[42] K. Sato, T. Shiba, J.I. Anzai, Polymers 5 (2013) 696–705.
[43] R. Watanabe, T. Sakamoto, K. Yamazoe, et al., Angew. Chem. Int. Ed. 59 (2020) 23461–23465.
[44] I. Stenina, D. Golubenko, V. Nikonenko, A. Yaroslavtsev, Int. J. Mol. Sci. 21 (2020) 5517.
[45] I.A. Stenina, A.B. Yaroslavtsev, Membranes 11 (2021) 198.